Stability and Exfoliation of Germanane: A Germanium Graphane Analogue

Elisabeth Bianco,[†] Sheneve Butler,[†] Shishi Jiang,[†] Oscar D. Restrepo,[‡] Wolfgang Windl,[‡] and Joshua E. Goldberger[†,*]

[†]Department of Chemistry and Biochemistry, The Ohio State University, Columbus, Ohio 43210-1340, United States and [‡]Department of Materials Science and Engineering, The Ohio State University, Columbus, Ohio 43210-1340, United States. The manuscript was written through contributions of all authors. Synthesis, XRD, and IR/Raman characterization of GeH were collected by E.B. and S.J. XPS measurements were collected by S.B. Single-layer germanane sheets were prepared and imaged by S.B.O.R., and W.W. performed the theoretical simulations. All experiments and concepts were designed by J.G. All authors have given approval to the final version of the manuscript.

ABSTRACT Graphene's success has shown not only that it is possible to create stable, single-atom-thick sheets from a crystalline solid but that these materials have fundamentally different properties than the parent material. We have synthesized for the first time, millimeter-scale crystals of a hydrogen-terminated germanium multilayered graphane analogue (germanane, GeH) from the topochemical deintercalation of $CaGe_2$. This layered van der Waals solid is analogous to multilayered graphane (CH). The surface layer of GeH only slowly oxidizes in air over the span of 5 months, while the underlying layers are resilient to oxidation based on X-ray photoelectron spectroscopy and Fourier transform infrared spectroscopy measurements. The GeH is thermally stable up to 75 °C; however, above this temperature amorphization and dehydrogenation begin to occur. These sheets can be mechanically exfoliated as single and few layers onto SiO_2/Si surfaces. This material represents a new class of covalently terminated graphane analogues and has great potential for a wide range of optoelectronic and sensing applications, especially since theory predicts a direct band gap of 1.53 eV and an electron mobility *ca.* five times higher than that of bulk Ge.

KEYWORDS: 2D materials · graphene analogues · layered materials · germanium · germanane · hydrogenated germanene

The discovery of single-layer graphene has shown not only that it is possible to create stable single-atom-thick layers from anisotropic crystal structures held together mainly *via* weak van der Waals interactions but that these isolated layers can have fundamentally different electronic structures and properties from the parent material.[1,2] For example, in a single layer of graphene electrons behave as massless Dirac fermions, resulting in potential applications for sensors, high-mobility transistors, transparent conducting electrodes, and photocatalyst supports.[3−5] This has sparked much recent interest toward understanding how the bulk properties of other layered van der Waals bonded crystal structures (MoS_2, WS_2, Bi_2Se_3, BN, *etc.*) change when prepared as isolated individual sheets.[6,7] For example, bulk MoS_2 normally has an indirect band gap at 1.29 eV, whereas isolated single layers of MoS_2 have a direct gap (1.8 eV).[8−10] Single layers of MoS_2 have also attracted much interest as high-mobility transistors.[10]

Most of the layered materials studied to date are composed of neutral or ionic layers and lack the possibility for chemical functionalization. Designing electronically active layers that could be covalently modified without disrupting the electronically relevant state would be incredibly advantageous for a wide range of applications. The nature of this terminal substituent not only would potentially give a synthetic handle for tuning the entire electronic structure based on its identity and electron-withdrawing capability but could also enable the grafting of functional ligands for high-specificity sensing applications. Graphene can be grafted with organic components, oxidized, or even terminated with hydrogen atoms to form graphane (CH);[11,12] however, these modifications disrupt the excellent carrier mobility in graphene and also are not stable long-term.[13] Other group IV layered lattices may maintain appreciable conductivity when the atoms are in the sp^3-hybridized state. Recently, single-layer-thick

* Address correspondence to goldberger@chemistry.ohio-state.edu.

Received for review February 24, 2013 and accepted March 18, 2013.

Published online March 19, 2013
10.1021/nn4009406

sp^2 and sp^3 group IV systems have attracted considerable theoretical and experimental interest.[14−17]

It has been previously shown that layered Zintl phases such as $CaSi_2$ and $CaGe_2$ can be topochemically deintercalated in aqueous HCl at low temperatures to produce layered silicon and germanium solids.[18−20] The resultant four-coordinate puckered lattice of Si and Ge atoms has an analogous geometry to sp^3-hybridized graphane or a Si/Ge(111) surface in which every Si/Ge atom is terminated with either −H or −OH above or below the layer.[18,21] There is a great propensity for the silicon lattice to oxidize, initially forming siloxene ($SiH_{0.5}(OH)_{0.5}$) sheets that are terminated with either Si−H or Si−OH bonds at the fourth coordination site, which eventually degrade to form SiO_2 under ambient conditions.[20,22] Appreciable Si−OH bond formation is always observed in the Fourier transform infrared spectroscopy (FTIR) spectrum as an intense, broad Si−O stretching mode at 1000−1200 cm^{-1}, even after HF treatment.[20] In contrast, the air and thermal stability of germanane (GeH) has not been rigorously characterized. Resistance to oxidation is an essential prerequisite for many future applications. From previous work,[18] there remain questions about the structure, air stability, thermal stability, and crystallinity of bulk GeH, as characterization did not include transmission electron microscopy, Raman spectroscopy, and X-ray photoelectron spectroscopy (XPS) data. Additionally, while previous work focused on interconverting micrometer-thick epitaxial thin films of $CaGe_2$ on Ge(111) into GeH, the present study focuses on the synthesis of free-standing crystals of $CaGe_2$. Furthermore, the exfoliation of single- and few-layer sheets of GeH has yet to be shown.

Herein, we demonstrate for the first time the gram-scale synthesis of millimeter-scale crystals of a layered GeH van der Waals solid that have platelet-like morphologies akin to Kish graphite. We prove by FTIR and XPS measurements that the surface layer of GeH slowly oxidizes in air over the span of 5 months, while the underlying layers resist oxidation. GeH is thermally stable up to 75 °C, above which amorphization begins to occur. Amorphization is complete at 175 °C, and dehydrogenation occurs from 200 to 250 °C. We show that the layered GeH has an observed band gap at 1.59 eV and also demonstrate the exfoliation of single and few layers onto SiO_2/Si substrates. Finally, we perform high-level theory calculations of the electronic structure that predict the effective masses, mobilities, and band gap of bulk and single-layer germanane.

RESULTS AND DISCUSSION

We synthesized hydrogen-terminated germanane by the topotactic deintercalation of β-$CaGe_2$ in aqueous HCl at −40 °C for at least 8 days (Figure 1). Crystals (2−6 mm) of β-$CaGe_2$ were first synthesized by sealing stoichiometric ratios of Ca and Ge in a quartz tube,

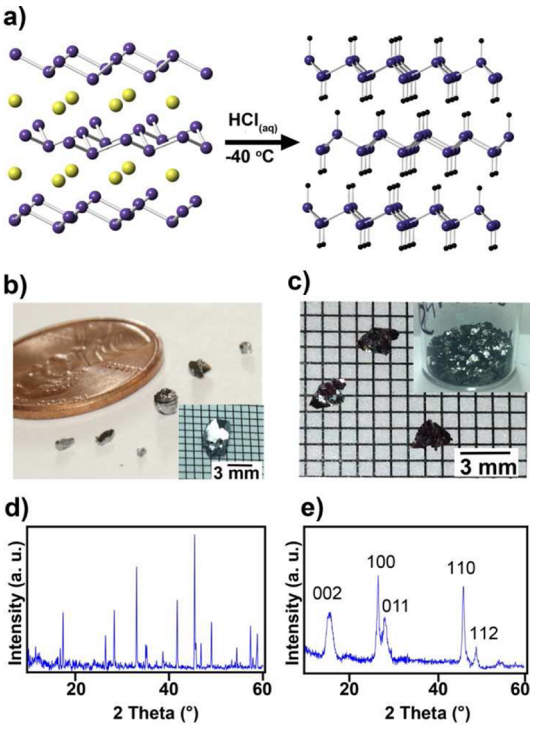

Figure 1. (a) Schematic illustration of topotactic deintercalation of $CaGe_2$ to GeH. Optical images of (b) $CaGe_2$ and (c) GeH crystals with select crystals on graph paper with a 1 mm grid (inset). Powder XRD pattern of (d) $CaGe_2$ and (e) GeH.

annealing to 950−1050 °C, and cooling over a period of 2−10 days (Figure 1b). High-purity $CaGe_2$ was confirmed *via* powder X-ray diffraction (Figure 1d). After HCl treatment, the product was filtered and washed with methanol to remove residual $CaCl_2$, yielding crystallites of GeH that are 2−3 mm in diameter and <100 μm in thickness (Figure 1c). X-ray diffraction analysis of GeH confirms that it can be fit to a 2H unit cell (2 GeH layers per hexagonal *c*-unit cell spacing) with a = 3.880 Å and c = 11.04 Å (5.5 Å per layer). Compared to the original $CaGe_2$ unit cell parameters of a = 3.987 Å, c = 30.0582 Å (six-layer stacking, $c/6$ = 5.097 Å), the hydrogen-terminated germanane is slightly contracted in the *a*-direction but expanded in the *c*-direction due to the replacement of Ca^{2+} with two Ge−H bonds between each layer. These lattice parameters do not correspond to any of the previously reported allotropes of germanium.[23,24] The narrower full-width-half-maximum (fwhm) of the (100) and (110) diffraction reflections (~0.4° 2θ) compared to the (002), (011), and (112) peaks (~1.3° 2θ) indicates that there is a significant amount of disorder along the *c*-axis, which is common in layered materials. This disorder along the *c*-axis precludes further structure determination *via* Rietveld analysis.

Transmission electron microscopy analysis indicates the product has a layered morphology with individual layers having less contrast than the 10 nm lacey carbon support grid (Figure 2a,b). The energy dispersive X-ray

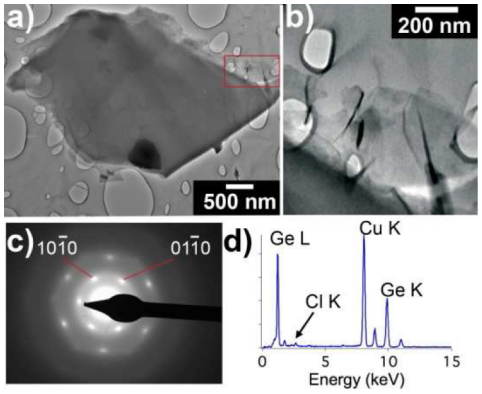

Figure 2. (a) Low-magnification and (b) magnified TEM micrograph of GeH platelets. (c) Electron diffraction pattern of platelets collected down the 0001 zone axis. (d) Energy dispersive X-ray spectroscopy of the GeH sheets.

spectrum has a strong Ge signal, an absence of Ca and O signals, and the presence of trace amounts of Cl. The Cl:Ge ratio was estimated to be 2:98 (Figure 2d). Figure 2c is an electron diffraction pattern taken orthogonal to the layers, showing a hexagonal arrangement of diffraction peaks that occur in the *a*- and *b*-directions. These data further confirm that the crystallinity of the germanium layered framework is preserved upon HCl treatment, and there is a strong registration in the stacking between each layer. The GeH electron diffraction pattern can be indexed to a simple hexagonal unit cell with $a = b \approx 3.87$ Å, assuming a [001] zone axis.

To further confirm hydrogen termination, we performed FTIR, Raman spectroscopy, and XPS on the germanane product (Figure 3). Transmission mode FTIR of samples ground up and pressed into KBr pellets shows extremely strong Ge−H stretching and multiple wagging modes at ∼2000 cm^{-1} and 570, 507, and 475 cm^{-1}, respectively. Additionally, weak vibrational modes at 770 and 825 cm^{-1} are also observed. These two vibrations also occur in the spectra of amorphous $Ge_{0.7}$:$H_{0.3}$ thin films and have been assigned by M. Cardona *et al.* to originate from bond-bending Ge−H_2 modes from nearest neighbor Ge atoms.[25,26] Thus, we hypothesize that these vibrations correspond to Ge−H_2 bond-bending modes from neighboring Ge atoms at the edges of each crystalline germanane sheet and/or to Ge−H_2 bonds within the lattice arising from Ge vacancies. We do not observe the presence of the broad, intense Ge−O—Ge and Ge−O vibrational modes that occur between 800 and 1000 cm^{-1}.[27] To confirm that these vibrational modes originate from Ge−H_2 and not Ge−O−Ge, we prepared GeD by treating $CaGe_2$ in 95% deuterated DCl/D_2O and collected the FTIR spectrum (Figure S1). The 825 and 770 cm^{-1} vibrational modes almost completely disappear, and new Ge−D_2 modes at 586 and 514 cm^{-1} appear along with residual Ge−H wagging modes. This is generally consistent with the change in reduced

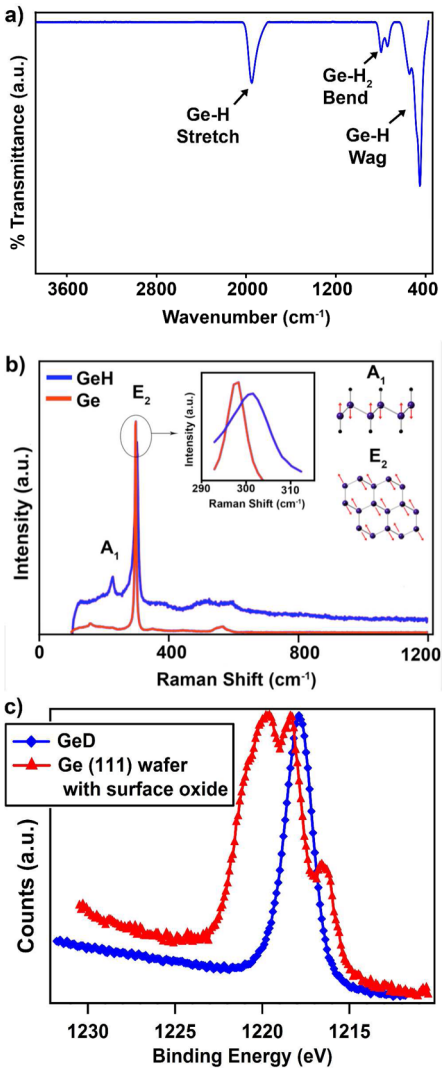

Figure 3. (a) Transmission-mode FTIR of GeH. (b) Raman spectrum of GeH (red) and Ge powder (blue), highlighting the difference in energy of the E_2 peak between GeH and Ge (middle inset), as well as a schematic illustration of the A_1 and E_2 vibrational modes. (c) XPS spectrum of the Ge 2p peak for GeH and a Ge(111) wafer with native surface oxide.

mass upon deuteration, and these vibrational frequencies are also apparent in amorphous $Ge_{0.7}$:$D_{0.3}$ films.[25]

From Raman spectroscopy (Figure 3b), the main Ge−Ge stretch in GeH occurs at 302 cm^{-1}, which is slightly blue-shifted compared to the 297 cm^{-1} E_2 Raman mode for crystalline germanium. In addition, a second vibrational mode emerges at 228 cm^{-1}. We performed *ab initio* calculations of the Γ-point phonon modes in GeH using Perdew−Burke−Ernzerhof (PBE) functionals as implemented in VASP.[27,28] These calculations predict the presence of Ge-based A_1 and E_2 Raman modes (assuming a C_{6v} point group) that occur at 223 and 289 cm^{-1}, respectively, which are in good agreement with the observed Raman modes. The symmetries of the vibrational modes are shown in the Figure 3b inset.

XPS measurements are also indicative of a single germanium oxidation state. XPS analysis of the Ge 2p3/2

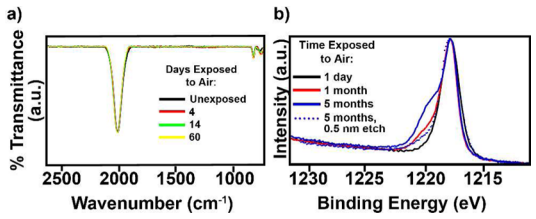

Figure 4. (a) Time-dependent reflection mode FTIR of a GeH platelet after exposure to ambient atmosphere for up to 60 days, collected *via* reflection mode, highlighting minimal changes in the relative intensity of the Ge−H to Ge−O vibrations. (b) Time-dependent XPS spectra of germanane immediately after exposure to atmosphere, after 1 day, and after 5 months, followed by Ar etching by 0.5 nm.

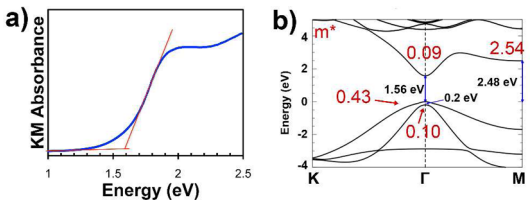

Figure 5. (a) DRA spectrum of GeH plotted as($h\nu\alpha$ *vs* photon energy highlighting a 1.59 eV band gap. The large tail at lower energies. (b) Electronic band structure of an isolated single layer of GeH calculated using HSE-06 theory including spin−orbit coupling predicting a 1.56 eV direct band gap. The hole and electron effective masses for each extrema are indicated in red.

peak for GeH shows a single peak at 1217.8 eV, which is indicative of Ge^{+}. A shift in the Ge 2p3/2 peak energy from Ge^{0} (1217.0 eV) is expected since hydrogen is more electronegative than germanium (Figure 3c). A control Ge(111) wafer with surface oxide shows a mixture of germanium oxidation states ranging from Ge^{0} (1217.0 eV) to Ge^{2+} (1218.9 eV) to Ge^{4+} (1221.4 eV).

The potential utility of germanane for any optoelectronic or sensing device strongly hinges on its air and temperature stability. Some previous reports state that hydrogen-terminated Ge(111) surfaces having the same atomic configuration as GeH are resistant to oxidation when the Ge surface has minimal defects, although some debate remains.[27−29] Because FTIR spectroscopy is an extremely sensitive probe of the presence of Ge−O and Ge−H bonds, we conducted a time-dependent FTIR study to determine if Ge−O vibrational modes in the 800−1000 cm^{-1} range emerge after exposure to an ambient atmosphere. After 60 days we observed virtually no change in this range, thus proving that the bulk of GeH resists oxidation (Figure 4a). Additionally, time-dependent XPS was performed to probe changes in the Ge oxidation state of the surface after exposing these layered GeH crystals to air (Figure 4b), and the percentage of each germanium oxidation state for all spectra was calculated by applying a standard Gaussian fit. After 1 month of exposure to air, a $Ge^{2+/3+}$ shoulder emerges at ~1219.3 eV (19.5% $Ge^{2+/3+}$). This peak becomes more intense after 5 months of air exposure (29.7% $Ge^{2+/3+}$). After Ar etching the top 0.5 nm (<1 layer), the $Ge^{2+/3+}$ almost completely disappears with 10.1% $Ge^{2+/3+}$ remaining. Together, the XPS and FTIR suggest that only the surface becomes oxidized over time.

The optical properties of germanane were investigated by diffuse reflectance absorption (DRA) spectroscopy. The silver-black material has a broad absorption over visible wavelengths, and a linear approximation of the absorption edge suggests a band gap of approximately 1.59 eV (Figure 5a). The Tauc/Davis-Mott expression for materials with 2D densities of states predicts that the absorbance $A(\hbar\omega)$ at photon energy $\hbar\omega$ near the band edge would be a step function with a discontinuity in absorbance at the band gap if the band gap was direct allowed. If the band gap was indirect allowed, the absorbance would be proportional to $\hbar\omega - E_g' \pm E_p$, where E_g' is the indirect gap and E_p is the energy of a particular phonon mode. However, it has been experimentally established that the Tauc/Davis-Mott approximations of absorption cannot unambiguously determine the transition mechanism for fundamental absorption for bulk materials with 2D densities of states.[9,30,31] We modeled the absorbance assuming direct-allowed, direct-forbidden, indirect-allowed, and indirect-forbidden gaps using both 2D and 3D densities of states (Figure SI-2). All of these plots estimated fundamental gaps ranging from 1.48 to 1.60 eV. These analyses are complicated by a broad Urbach edge at the lower end of the absorption tail, which is often indicative of a large doping concentration or disorder. The presence of photoluminescence is often a stronger test of a direct band gap. Previously reported studies of GeH thin films proposed that GeH is a direct band gap material with a fundamental absorption gap at 1.8 eV based on photothermal deflection spectroscopy and photoluminescence that occurs at 0.45 eV lower, or 1.35 eV.[32] We did not observe any photoluminescence from 1.1 to 1.8 eV when exciting from 1.38 to 1.96 eV at temperatures ranging from 14 to 300 K. This lack of photoluminescence and linear slope in our samples might suggest that germanane has an indirect band gap. However, the lack of photoluminescence alone is not sufficient evidence of an indirect gap. A direct band gap material could lack photoluminescence if there is a large concentration of nonradiative defect states or impurities in the sample or if the material possesses unique surface or edge states. The presence of any of these can quench photoluminescence and also contribute to the observed bowed Urbach edge. Therefore, further optimization of the growth and etching chemistry will be necessary before dismissing the potential existence of a direct band gap. Also, we propose that more direct measurements, such as angle-resolved photoemission spectroscopy, as well as additional temperature-dependent absorption studies are necessary to completely conclude whether germanane has a direct or

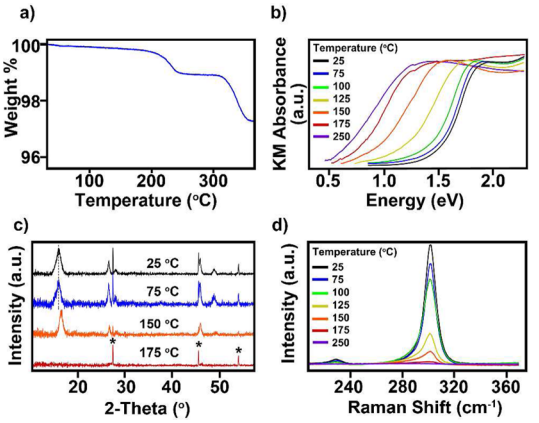

Figure 6. (a) TGA analysis of GeH. (b) DRA spectra, (c) XRD patterns, and (d) Raman spectra of GeH measured after 4 hour annealing treatments at various temperatures in 5% H_2/Ar. In (c) the starred peaks correspond to reflections of an internal Ge standard, and the dashed line is drawn to guide the eye.

indirect band gap, especially since our theory predicts GeH to have a direct band gap.

The temperature stability of germanane was also probed *via* thermogravimetric analysis (TGA), DRA, XRD, and Raman upon annealing at a range of temperatures in 5% H_2/Ar. TGA shows a ~1.1% mass loss at 200−250 °C, which is close to the expected mass loss of 1 equivalent of hydrogen in GeH, as well as a 1.7% mass loss of that occurs between 320 and 355 °C (Figure 6a). This second mass loss likely corresponds to the loss of Cl (3.6% molar). X-ray fluorescence analysis further supports this, as there is approximately a 1 order of magnitude decrease in the chlorine intensity after annealing at 375 °C. Furthermore, it has been reported in previous temperature-programmed desorption studies that Cl desorbs off of germanium at temperatures ranging from 300 to 350 °C.[33] However, there is a significant change in the absorption spectrum when annealing at temperatures above 75 °C. The absorption onset, as detected by DRA, red shifts by 0.06 eV upon annealing at 75 °C (Figure 6b). The absorption profile continues to red-shift with higher temperature annealing until 250 °C, when the absorption onset (0.58 eV) goes below that of bulk germanium (0.67). Previously studies have reported that amorphous Ge thin films have band gaps lower than that of bulk germanium (0.50 *vs* 0.67 eV)[34] and amorphous hydrogenated germanium films have larger band gaps (1.1 eV).[35] There is no obvious change in the XRD patterns (Figure 6c) until 150 °C, at which point the *c*-axis decreases from $c = 11.04$ Å to $c = 10.70$ Å and the fwhm of this 002 reflection decreases from 1.3° 2θ to 0.8° 2θ. The diffraction pattern shows complete amorphization upon annealing at 175 °C. Raman spectroscopy shows a consistent decrease in the intensity of both the Ge−Ge and Ge−H modes as a function of annealing temperature (Figure 6d). After 175 °C, there is ~2 order magnitude decrease in the Raman scattering intensity of both the E_2 and A_1 modes. Taken together, this suggests that amorphization occurs at temperatures well below that of dehydrogenation (200−250 °C). We hypothesize that the low-temperature amorphization, the broadness of the 00*l* reflections, and the lack of observed photoluminescence are consequences of the presence of trace percentages of Ge−Cl bonds. If regions with a high concentration of Ge−Cl bonds amorphize first, this would explain the observed decrease in the *c*-parameter and fwhm of the 00*l* reflections at 150 °C. The observed diffraction pattern at this temperature is indicative of local domains of pure GeH that did not undergo amorphization due to the lack of nearby chlorine. This hypothesis will be the basis of future investigations.

Band structure calculations suggest that germanane is a direct band gap material both as isolated layers and in the crystal structure having two layers per unit cell. We used the density functional theory (DFT) code VASP[36,37] to optimize the geometry and calculate the band structure of isolated single layer and two-layer unit cell GeH. The interactions between cores and electrons were described for relaxation by projector augmented wave (PAW) pseudopotentials[38] within the PBE exchange−correlation function[39,40] with a plane-wave cutoff energy of 600 eV. van der Waals interactions between the layers were included using the DFT-D2 method by Grimme.[41] For the two-layer structure, the unit cell was modeled as a $P6_3mc$ unit cell with relaxed lattice parameters of $a = 4.05$ Å and $c = 10.56$ Å, thus having a 5.3 Å layer spacing. For the isolated single-layer structure, our calculations were performed in a unit cell with 20 Å of additional vacuum between GeH layers. To obtain an accurate description of the band gap in this system, we utilized the hybrid HSE06[42−44] exchange−correlation function. With this function we obtain a direct gap at the Γ point of 1.56 eV for an isolated layer (Figure 5b) and 1.53 eV for the two-layer unit cell (Figure S3), which is in excellent agreement with the observed experimental band gap. The calculated band gap for the two-layer unit cell at the A point of the Brillouin zone is ~1.77 eV. The difference in energy between the conduction band minimum at the M point and the valence band maximum at Γ is 2.48 and 2.33 eV for an isolated layer and two-layer unit cell, respectively. In both cases, spin−orbit splitting at the Γ valence band maximum is 0.2 eV.

Additionally, the effective masses of the conduction and valence bands at each extremum were calculated for the isolated single layer and are shown in Figure 5b. In bulk crystalline germanium, the conduction band minima occur in the four equivalent valleys at the L ⟨111⟩ point, which have much higher effective mass ($m_{eL}^* = 1.64$) than the conduction band valleys at Γ ($m_{e\Gamma}^* = 0.041$).[45] However, since GeH can be thought of as hydrogen-terminated isolated (111) sheets of

germanium, we are effectively eliminating the L wavevector in the Brillouin zone. We calculated from first-principles[46,47] the phonon-limited electronic mobility for an isolated single layer, obtaining a high mobility of 18 195 $cm^2/(V\ s)$. This 5× increase in electron mobility from bulk Ge (3900 $cm^2/(V\ s)$) is consistent with the reduced electron effective mass in GeH.

Also, using the EXCITING-CODE, we solved the Bethe–Salpeter equation to account for the excitonic effects.[48] We used the scissors operator to obtain a band gap of 1.53 eV for the two-layer unit cell (to match our HSE-calculated band gap value). Within this theoretical framework we calculated an excitonic binding energy of 0.28 eV for the two-layer unit cell. Pulci *et al.*[49] used the GW approximation to calculate the ground state of germanane. They found a much larger direct quasi-particle band gap of 2.4 eV, far outside of the experimental range established here. They reported an excitonic peak with a higher binding energy of 0.6 eV below the conduction band. The difference between Pulci's exciton binding energy and our reported value agrees with the fact that our smaller band gap provides a larger screening that can decrease the exciton binding energy. No excitonic phenomena were observed in the absorption or photoluminescence of our samples. However, this 0.28 eV exciton binding energy may explain the previously observed 0.45 eV red shift between the absorption onset and photoluminescence of epitaxial GeH thin films.[32]

Finally, we demonstrate that hydrogen-terminated germanane can be mechanically exfoliated into single sheets. As with most other layered crystal structures, the GeH crystal structure is held together mainly *via* van der Waals bonding. By incorporating van der Waals corrections into the PBE simulation, the interlayer binding energy for GeH was found to be nearly entirely dominated by van der Waals interaction with a value of 72 meV per Ge atom, in the same range as the calculated 53.5 meV per C atom in graphite.[41] We therefore used both Scotch tape and polydimethylsiloxane to exfoliate few- and single-layer-thick sheets onto Si substrates with a wide range of SiO_2 thicknesses (100–165, 275–345 nm) to attain maximum contrast by optical microscopy. Few-layer and single-layer sheets were visible by optical microscopy, with 110 and 300 nm thick SiO_2 substrates providing optimal contrast. Figure 7a shows an AFM image, optical micrograph, and corresponding height profile for a 6–7-layer-thick germanane flake. Figure 7b shows an AFM image, optical micrograph, and the corresponding height profile for a 2 μm × 2 μm single GeH layer

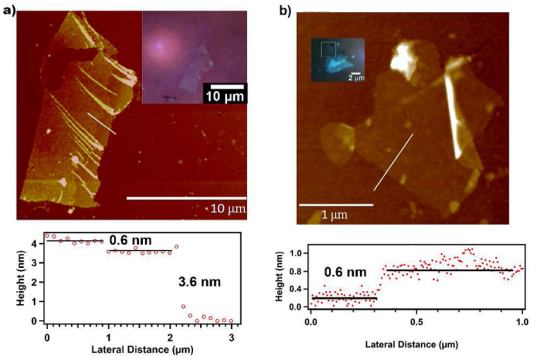

Figure 7. (a) AFM micrograph (top), height profile (bottom), and optical micrograph (inset) of few-layer GeH deposited on 110 nm SiO_2/Si. (b) AFM micrograph (top) and height profile (bottom) of single-layer-thick GeH sheet.

exfoliated onto a 100 nm thick SiO_2/Si substrate. The observed height (~6 Å) agrees well with the expected value of 5.5 Å for a single layer, since it is well known that differences in the attractive potentials between the AFM tip, the substrate, and the layered material often cause the measured AFM thickness to be larger than the expected value.[50] The weak Raman intensities of few-layer GeH, the photothermal degradation at laser intensities above 40 kW/cm^2, and the overlap of the two E_2 and A_1 Raman modes with higher order silicon substrate Raman modes prevent the collection of thickness-dependent Raman maps on conventional SiO_2/Si substrates. Regardless, our ability to produce single- and few-layer-thick germanane sheets with >2 μm length and width will enable further study of the layer dependence on the vibrational, optical, and electronic properties.

CONCLUSIONS

In summary, we have created gram-scale, millimeter-sized crystallites of hydrogen-terminated germanane and have characterized for the first time their long-term resistance to oxidation and thermal stability, a necessary prerequisite for any practical application. We have also demonstrated the ability to exfoliate single- and few-layer sheets on surfaces, thus creating a germanium framework analogous to graphane. Theory predicts that the created material has a direct band gap of 1.55 eV with low effective masses, thus strongly increasing the already high carrier mobilities found in Ge without the penalty of the low bulk gap. This notion of creating dimensionally reduced molecular-scale "allotropes" of materials with fundamentally different and potentially transformative properties compared to the bulk can be clearly expanded beyond carbon.

METHODS

Synthesis. In a typical reaction, Ca and Ge were loaded in stoichiometric amounts into a quartz tube and evacuated on a Schlenk line to milliTorr pressures. The quartz tube was sealed under vacuum using a hydrogen–oxygen torch, annealed at 950–1050 °C for 16–20 h, and cooled to room temperature

over 1−5 days. Germanium (Ge, 99.999%, Acros) and calcium (Ca, 99%, Acros) were purchased and used without further purification. To synthesize GeH, $CaGe_2$ crystals were stirred in concentrated HCl(aq) for 5−10 days at −40 to −20 °C. To purify GeH, the GeH product was washed with Milli-Q H_2O followed by methanol, then dried at room temperature on a Schlenk line.

Measurements. Powder X-ray diffraction was collected on a Bruker D8 powder X-ray diffractometer. FTIR and time-dependent FTIR measurements were collected on a Perkin-Elmer Frontier Dual-Range FIR/MidIR spectrometer that was loaded in an Ar-filled glovebox. Raman scattering spectra were collected using a Renishaw InVia Raman equipped with a CCD detector. The Raman spectra were collected using 633 nm (He−Ne red laser) and 785 nm (near-IR diode laser) illumination. XPS was collected using a Kratos Axis Ultra X-ray photoelectron spectrometer equipped with a monochromated (Al) X-ray gun. The Ar ion etch rate was calibrated using SiO_2. AFM images were collected on a Bruker 3000 scanning probe microscope with a Nanoscope IIIa controller. X-ray fluorescence measurements were performed using an Olympus DELTA hand-held X-ray fluorescence analyzer. TGA was performed using a TA Instruments Q-500 thermogravimetric analyzer. Samples were analyzed from room temperature to 375 °C at a ramp rate of 10 °C/min under a flowing N_2 atmosphere. Diffuse reflectance absorption measurements were conducted using a CARY 5000 UV/vis NIR spectrophotometer, with a diffuse reflectance integrating sphere attachment.

Conflict of Interest: The authors declare no competing financial interest.

Supporting Information Available: GeD FTIR spectrum, simulated band structure of two layers per unit cell GeH, and additional single-layer GeH AFM data. This material is available free of charge *via* the Internet at http://pubs.acs.org.

Acknowledgment. The authors acknowledge the generosity of G. Natu, Y. H. Liu, and Prof. Y. Wu for DRA absorption measurements. This work was supported in part by an allocation of computing time from the Ohio Supercomputing Center. We also acknowledge the Analytical Surface Facility at OSU chemistry, supported by National Science Foundation under grant number CHE-0639163. We also acknowledge The Ohio State University Undergraduate Instrumental Analysis Program for the use of their instrumentation. This project was supported by the National Science Foundation under project number DMR-1201953, the Army Research Office (W911-NF-12-1-0481), the Center for Emergent Materials at The Ohio State University, an NSF MRSEC at The Ohio State University (Grant DMR-0820414), The Ohio State University Materials Research Seed Grant Program, and startup funding from The Ohio State University.

REFERENCES AND NOTES

1. Novoselov, K. S.; Geim, A. K.; Morozov, S. V.; Jiang, D.; Katsnelson, M. I.; Grigorieva, I. V.; Dubonos, S. V.; Firsov, A. A. Two-Dimensional Gas of Massless Dirac Fermions in Graphene. *Nature* **2005**, *438*, 197–200.
2. Novoselov, K. S.; Geim, A. K.; Morozov, S. V.; Jiang, D.; Zhang, Y.; Dubonos, S. V.; Grigorieva, I. V.; Firsov, A. A. Electric Field Effect in Atomically Thin Carbon Films. *Science* **2004**, *306*, 666–669.
3. Fowler, J. D.; Allen, M. J.; Tung, V. C.; Yang, Y.; Kaner, R. B.; Weiller, B. H. Practical Chemical Sensors from Chemically Derived Graphene. *ACS Nano* **2009**, *3*, 301–306.
4. Liang, Y.; Li, Y.; Wang, H.; Zhou, J.; Wang, J.; Regier, T.; Dai, H. Co_3O_4 Nanocrystals on Graphene as a Synergistic Catalyst for Oxygen Reduction Reaction. *Nat. Mater.* **2011**, *10*, 780–786.
5. Williams, G.; Seger, B.; Kamat, P. V. TiO_2-Graphene Nanocomposites. UV-Assisted Photocatalytic Reduction of Graphene Oxide. *ACS Nano* **2008**, *2*, 1487–1491.
6. Novoselov, K. S.; Jiang, D.; Schedin, F.; Booth, T. J.; Khotkevich, V. V.; Morozov, S. V.; Geim, A. K. Two-Dimensional Atomic Crystals. *Proc. Natl. Acad. Sci.* **2005**, *102*, 10451–10453.
7. Ci, L.; Song, L.; Jin, C.; Jariwala, D.; Wu, D.; Li, Y.; Srivastava, A.; Wang, Z. F.; Storr, K.; Balicas, L.; *et al*. Atomic Layers of Hybridized Boron Nitride and Graphene Domains. *Nat. Mater.* **2010**, *9*, 430–435.
8. Lee, C.; Yan, H.; Brus, L. E.; Heinz, T. F.; Hone, J.; Ryu, S. Anomalous Lattice Vibrations of Single- and Few-Layer MoS_2. *ACS Nano* **2010**, *4*, 2695–2700.
9. Mak, K. F.; Lee, C.; Hone, J.; Shan, J.; Heinz, T. F. Atomically Thin MoS_2: A New Direct-Gap Semiconductor. *Phys. Rev. Lett.* **2010**, *105*, 136805.
10. Radisavljevic, B.; Radenovic, A.; Brivio, J.; Giacometti, V.; Kis, A. Single-Layer MoS_2 Transistors. *Nat. Nanotechnol.* **2011**, *6*, 147–150.
11. Elias, D. C.; Nair, R. R.; Mohiuddin, T. M. G.; Morozov, S. V.; Blake, P.; Halsall, M. P.; Ferrari, A. C.; Boukhvalov, D. W.; Katsnelson, M. I.; Geim, A. K.; *et al*. Control of Graphene's Properties by Reversible Hydrogenation: Evidence for Graphane. *Science* **2009**, *323*, 610–613.
12. Lomeda, J. R.; Doyle, C. D.; Kosynkin, D. V.; Hwang, W.-F.; Tour, J. M. Diazonium Functionalization of Surfactant-Wrapped Chemically Converted Graphene Sheets. *J. Am. Chem. Soc.* **2008**, *130*, 16201–16206.
13. Becerril, H. A.; Mao, J.; Liu, Z.; Stoltenberg, R. M.; Bao, Z.; Chen, Y. Evaluation of Solution-Processed Reduced Graphene Oxide Films as Transparent Conductors. *ACS Nano* **2008**, *2*, 463–470.
14. Feng, B.; Ding, Z.; Meng, S.; Yao, Y.; He, X.; Cheng, P.; Chen, L.; Wu, K. Evidence of Silicene in Honeycomb Structures of Silicon on Ag(111). *Nano Lett.* **2012**, *12*, 3507–3511.
15. Lew Yan Voon, L. C.; Sandberg, E.; Aga, R. S.; Farajian, A. A. Hydrogen Compounds of Group-IV Nanosheets. *Appl. Phys. Lett.* **2010**, *97*, 163114.
16. Ni, Z.; Liu, Q.; Tang, K.; Zheng, J.; Zhou, J.; Qin, R.; Gao, Z.; Yu, D.; Lu, J. Tunable Bandgap in Silicene and Germanene. *Nano Lett.* **2012**, *12*, 113–118.
17. O'Hare, A.; Kusmartsev, F. V.; Kugel, K. I. A Stable "Flat" Form of Two-Dimensional Crystals: Could Graphene, Silicene, Germanene Be Minigap Semiconductors? *Nano Lett.* **2012**, *12*, 1045–1052.
18. Vogg, G.; Brandt, M. S.; Stutzmann, M. Polygermyne−A Prototype System for Layered Germanium Polymers. *Adv. Mater.* **2000**, *12*, 1278–1281.
19. Okamoto, H.; Kumai, Y.; Sugiyama, Y.; Mitsuoka, T.; Nakanishi, K.; Ohta, T.; Nozaki, H.; Yamaguchi, S.; Shirai, S.; Nakano, H. Silicon Nanosheets and Their Self-Assembled Regular Stacking Structure. *J. Am. Chem. Soc.* **2010**, *132*, 2710–2718.
20. Dahn, J. R.; Way, B. M.; Fuller, E.; Tse, J. S. Structure of Siloxene and Layered Polysilane (Si_6H_6). *Phys. Rev. B* **1993**, *48*, 17872–17877.
21. Kautsky, H.; Herzberg, G. Concerning Siloxane and Its Derivatives. *Zeit. Anorg. Allgem. Chem.* **1924**, *139*, 135–160.
22. Yamanaka, S.; Matsuura, H.; Ishikawa, M. New Deintercalation Reaction of Calcium from Calcium Disilicide. Synthesis of Layered Polysilane. *Mater. Res. Bull.* **1996**, *31*, 307–316.
23. Faessler, T. F. Germanium(cF136): A New Crystalline Modification of Germanium with the Porous Clathrate-II Structure. *Angew. Chem., Int. Ed.* **2007**, *46*, 2572–2575.
24. Kiefer, F.; Karttunen, A. J.; Doblinger, M.; Fassler, T. F. Bulk Synthesis and Structure of a Microcrystalline Allotrope of Germanium (m-allo-Ge). *Chem. Mater.* **2011**, *23*, 4578–4586.
25. Bermejo, D.; Cardona, M. Infrared-Absorption in Hydrogenated Amorphous and Crystallized Germanium. *J. Non-Cryst. Solids* **1979**, *32*, 421–430.
26. Cardona, M. Vibrational-Spectra of Hydrogen in Silicon and Germanium. *Phys. Status Solidi B* **1983**, *118*, 463–481.
27. Rivillon, S.; Chabal, Y. J.; Amy, F.; Kahn, A. Hydrogen Passivation of Germanium (100) Surface Using Wet Chemical Preparation. *Appl. Phys. Lett.* **2005**, 87.
28. Deegan, T.; Hughes, G. An X-ray Photoelectron Spectroscopy Study of the HF Etching of Native Oxides on Ge(111) and Ge(100) Surfaces. *Appl. Surf. Sci.* **1998**, *123*, 66–70.
29. Bodlaki, D.; Yamamoto, H.; Waldeck, D. H.; Borguet, E. Ambient Stability of Chemically Passivated Germanium Interfaces. *Surf. Sci.* **2003**, *543*, 63–74.
30. Lee, P. A.; Said, G.; Davis, R.; Lim, T. H. On Optical Properties of Some Layer Compounds. *J. Phys. Chem. Solids* **1969**, *30*, 2719–2729.

31. Gaiser, C.; Zandt, T.; Krapf, A.; Serverin, R.; Janowitz, C.; Manzke, R. Band-Gap Engineering with HfS_xSe_{2-x}. *Phys. Rev. B* **2004**, *69*, 075205.
32. Vogg, G.; Meyer, A. J. P.; Miesner, C.; Brandt, M. S.; Stutzmann, M. Efficient Tunable Luminescence of SiGe Alloy Sheet Polymers. *Appl. Phys. Lett.* **2001**, *78*, 3956–3958.
33. Holman, Z. C.; Kortshagen, U. R. Nanocrystal Inks without Ligands: Stable Colloids of Bare Germanium Nanocrystals. *Nano Lett.* **2011**, *11*, 2133–2136.
34. Donovan, T. M.; Spicer, W. E.; Bennett, J. M. Evidence for a Sharp Absorption Edge in Amorphous Ge. *Phys. Rev. Lett.* **1969**, *22*, 1058–1061.
35. Chambouleyron, I.; Graeff, C. F.; Zanatta, A. R.; Fajardo, F.; Mulato, M.; Campomanes, R.; Comedi, D.; Marques, F. C. The Perspectives of Hydrogenated Amorphous Germanium as an Electronic Material. *Phys. Status Solidi B* **1995**, *192*, 241–251.
36. Kresse, G.; Hafner, J. *Veritio* Molecular-Dynamics for Liquid-Metals. *Phys. Rev. B* **1993**, *47*, 558–561.
37. Kresse, G.; Hafner, J. *Ab Initio* Molecular-Dynamics Simulation of the Liquid-Metal Amorphous-Semiconductor Transition in Germanium. *Phys. Rev. B* **1994**, *49*, 14251–14269.
38. Blochl, P. E. Projector Augmented-Wave Method. *Phys. Rev. B* **1994**, *50*, 17953–17979.
39. Perdew, J. P.; Burke, K.; Ernzerhof, M. Generalized Gradient Approximation Made Simple. *Phys. Rev. Lett.* **1996**, *77*, 3865–3868.
40. Perdew, J. P.; Burke, K.; Ernzerhof, M. Generalized Gradient Approximation Made Simple. *Phys. Rev. Lett.* **1997**, *78*, 1396.
41. Grimme, S. Semiempirical GGA-Type Density Functional Constructed with a Long-Range Dispersion Correction. *J. Comput. Chem.* **2006**, *27*, 1787–1799.
42. Heyd, J.; Scuseria, G. E.; Ernzerhof, M. Hybrid Functionals Based on a Screened Coulomb Potential. *J. Chem. Phys.* **2003**, *118*, 8207–8215.
43. Heyd, J.; Scuseria, G. E.; Ernzerhof, M. Hybrid Functionals Based on a Screened Coulomb Potential. *J. Chem. Phys.* **2006**, *124*, 219906.
44. Paier, J.; Marsman, M.; Hummer, K.; Kresse, G.; Gerber, I. C.; Angyan, J. G. Screened Hybrid Density Functionals Applied to Solids. *J. Chem. Phys.* **2006**, *125*, 249901.
45. *Landolt-Bornstein*; Madelung, O.; Schulz, M.; Weiss, H., Eds.; Springer: Berlin, 1987; Vol. 17a-h.
46. Restrepo, O. D.; Varga, K.; Pantelides, S. T. First-Principles Calculations of Electron Mobilities in Silicon: Phonon and Coulomb Scattering. *Appl. Phys. Lett.* **2009**, *94*, 212103.
47. Baroni, S. *Quantum ESPRESSO*, http://www.quantum-espresso.org/
48. Sagmeister, S.; Ambrosch-Draxl, C. Time-Dependent Density Functional Theory *versus* Bethe-Salpeter Equation: An All-Electron Study. *Phys. Chem. Chem. Phys.* **2009**, *11*, 4451–4457.
49. Pulci, O.; Gori, P.; Marsili, M.; Garbuio, V.; Del Sole, R.; Bechstedt, F. Strong Excitons in Novel Two-Dimensional Crystals: Silicane and Germanane. *EPL* **2012**, *98*, 37004.
50. Nemes-Incze, P.; Osvath, Z.; Kamaras, K.; Biro, L. P. Anomalies in Thickness Measurements of Graphene and Few Layer Graphite Crystals by Tapping Mode Atomic Force Microscopy. *Carbon* **2008**, *46*, 1435–1442.